Geometrical multiscale model of an idealized left ventricle with fluid-structure interaction effects coupled to a one-dimensional viscoelastic arterial network

Toni Lassila,* A. Cristiano I. Malossi,* Matteo Astorino,* and Simone Deparis*

* MATHICSE-CMCS, École Polytechnique Fédérale de Lausanne
EPFL, Station 8, CH-1015 Lausanne, Switzerland,
{toni.lassila,cristiano.malossi,matteo.astorino,simone.deparis}@epfl.ch

Abstract

A geometrical multiscale model for blood flow through an ideal left ventricle and the main arteries is presented. The blood flow in the three-dimensional idealized left ventricle is solved through a monolithic fluid-structure interaction solver. To account for the interaction between the heart and the circulatory system the heart flow is coupled through an ideal valve with a network of viscoelastic one-dimensional models representing the arterial network. The geometrical multiscale approach used in this work is based on the exchange of averaged/integrated quantities between the fluid problems. The peripheral circulation is modelled by zero-dimensional windkessel terminals. We demonstrate that the geometrical multiscale model is (i) *highly modular* in that component models can be easily replaced with higher-fidelity ones whenever the user has a specific interest in modelling a particular part of the system, (ii) *passive* in that it reaches a stable limit cycle of flow rate and pressure in a few heartbeat cycles when driven by a periodic force acting on the epicardium, and (iii) capable of operating at *physiological regimes*.

Keywords: left ventricle; fluid-structure interaction; hemodynamics; geometrical multiscale modelling; heterogeneous models.

Introduction

The accurate prediction of localized effects of therapeutic procedures on patients suffering from cardiovascular and arterial disease requires the simulation of the entire closed-loop system: the heart, the aorta, the arteries, the peripheral circulation, the veins, the lungs, and the pulmonary circulation. For this purpose many one-dimensional (1D) and zero-dimensional (0D) lumped parameter models for blood flow have been proposed in the literature – we refer to [24] for a recent review. While these models do well in capturing the essential phenomena of the flow, the concentrated parameters therein often have unclear physiological meaning and need to be calibrated based on patient-specific measurements before the models can produce physiological results. Therefore, when using such models it may be difficult to predict changes in a patient's physiology after a hypothetical surgery, since no measurements are a priori available for calibration.

With the advent of highly-scalable parallel CFD codes, full-fidelity three-dimensional (3D) fluid-structure interaction (FSI) simulations of localized compartments of the cardiovascular system have become feasible. In this framework, we recall for example the works [4, 12, 15], where 3D FSI simulations of important parts, namely the heart and the ascending aorta, have been reported. With respect to the reduced models, these high-fidelity models are characterized by more realistic physical laws and they can po-

tentially provide very accurate information on the complex physical phenomena that occur in the various compartments. From a practical point of view, however, a 3D FSI simulation of the whole cardiovascular system is characterized by excessive computational costs that would make such a simulation unfeasible even with the use of the most modern supercomputer.

From this perspective the geometrical multiscale model proposed in [8, 9], coupling together dimensionally heterogeneous models (3D, 1D, and 0D), offers a compromise between the two previous approaches (reduced models and 3D FSI). The use of 3D FSI models is therefore limited to specific regions of interest, where the 3D description of the domain plays an important role (e.g. in the heart and/or in the aortic arch etc.) in order to provide accurate information on the local physics. The remaining regions (i.e. the other major branches of the arterial tree) still rely on very cheap 1D models, which are perfectly suited for describing the waveform propagation along the arterial network. Finally, the model is completed by introducing lumped parameter models at the end of the arterial segments (representing the peripheral circulation) and for some other interface conditions (e.g. heart valves).

In this work the geometrical multiscale approach is adopted with a twofold objective: on the one hand to provide information on the global blood dynamics of the arterial system; on the other hand to accurately describe the lo-

cal FSI phenomena in the left ventricle. As a consequence, in our framework a system of 1D models and a 3D FSI model are used to describe the arterial tree and the left ventricle. From a mathematical and numerical point of view these heterogeneous computational models are coupled together by matching averaged/integrated quantities, namely the flow rate and the normal component of the traction vector, and the implicit coupling at each time step is achieved through nonlinear quasi-Newton iterations [14]. The geometrical multiscale framework has been implemented with the state-of-the-art parallel CFD code `LifeV` [5], and is highly modular and easily extensible to include more fine-scale constituent models.

Possible clinical applications involve pre- and/or post-surgical simulations of a pathological left ventricle, prediction of critical quantities such as cardiac output after the ventricle remodelling, and investigation of the influence of peripheral modifications of the arterial tree to the heart dynamics.

Physical models

Three-dimensional models. The 3D FSI model proposed here is adopted for simulation of the blood flow in the left ventricle. Despite the complexity of the blood rheology, a Newtonian incompressible fluid represents a suitable model for blood when we are not interested in the finer details of the flow [9]. The blood dynamics are therefore modelled by formulating the incompressible Navier–Stokes equations in the case of a moving fluid domain, resulting in the so-called Arbitrary Lagrangian Eulerian (ALE) formulation [17].

In order to describe the evolution of the fluid domain, the displacement of the endocardium (the inner surface of the ventricle) has to be recovered. Within this perspective two main approaches can be identified. A first possibility consists in reconstructing the displacement field from a suitable interpolation in space and time from a set of data points $\mathbf{h}(\mathbf{x}_i, t_j)$, $i = 1, \ldots, I$, $j = 1, \ldots, J$ obtained from medical images (see e.g. [19, 20]), followed by simulating only the fluid inside a moving ventricle. The second approach relies on an accurate mechanical simulation of the myocardium and on the corresponding numerical resolution of the coupled fluid-structure interaction problem, including possibly the eletrical activation of the heart. Both approaches have their own challenges. The former is computationally less expensive, but the straightforward prescription of time-dependent computational geometries reconstructed from medical images, which are often characterized by highly noisy data, may induce strong boundary singularities in the fluid solution (especially in the pressure field). The latter approach provides a smooth and (potentially) very accurate interface solution, but the mathematical model that characterizes heart tissue is often very complex and involves the description of important biological characteristics such as the fiber directions, the active and passive deformation, and the electric impulse [16, 18, 23].

In this work, we propose a different strategy, aiming at being a compromise between the two previous approaches. Rather than using the medical data to recover the displacement field of the endocardium, we focus on the reconstruction of the displacements of the epicardium, the outer surface Γ_{out}. The resulting field is then adopted as a boundary condition of a "simplified" structural model (here a linear elasticity model), which is eventually coupled with the fluid through the endocardium, now the fluid-structure interface Γ_{FSI}.

Remark. Note that in this approach the structural model adopted is a poor approximation of the true mechanical model. Its main purpose is to smooth the noisy data and transfer them onto Γ_{FSI}. It should therefore be understood that within this strategy we can not expect to recover any physiologically relevant information on the biological tissue, such as internal stresses. Ongoing work consists in extending this strategy to more complex mechanical models [22].

Let $\Omega = \Omega_{\mathrm{f}} \cup \Omega_{\mathrm{s}}$ be a reference configuration of the fluid-structure system, with Ω_{f} and Ω_{s} the reference domains for the fluid and the solid, respectively. We denote by $\Gamma_{\mathrm{FSI}} \stackrel{\mathrm{def}}{=} \partial\Omega_{\mathrm{f}} \cap \partial\Omega_{\mathrm{s}}$ the fluid-solid interface. The current configuration of the fluid domain, $\Omega_{\mathrm{f}}(t)$, is parametrized by the ALE map

$$
\begin{aligned}
\mathcal{A}_t : \Omega_{\mathrm{f}} &\to \Omega_{\mathrm{f}}(t) \\
\mathbf{x} &\mapsto \mathcal{A}_t(\mathbf{x}) = \mathbf{x} + \mathbf{d}_{\mathrm{f}}(\mathbf{x}),
\end{aligned}
\tag{1}
$$

as $\Omega_{\mathrm{f}}(t) = \mathcal{A}_t(\Omega_{\mathrm{f}}, t)$, where $\mathbf{d}_{\mathrm{f}} : \Omega_{\mathrm{f}} \times \mathbb{R}^+ \to \mathbb{R}^3$ are the displacement of the fluid domain. We denote by $\Gamma_{\mathrm{FSI}}(t) \stackrel{\mathrm{def}}{=} \partial\Omega_{\mathrm{f}}(t) \cap \partial\Omega_{\mathrm{s}}(t)$ the current position of the fluid-solid interface. In practice, $\mathbf{d}_{\mathrm{f}} = \mathrm{Ext}(\mathbf{d}|_{\Gamma_{\mathrm{FSI}}})$, where $\mathbf{d} : \Omega_{\mathrm{s}} \times \mathbb{R}^+ \to \mathbb{R}^3$ stands for the solid displacement and $\mathrm{Ext}(\cdot)$ denotes an harmonic lifting operator from Γ_{FSI} to Ω_{f}.

The nonlinear fluid-structure problem under consideration reads as follows (see e.g. [9, Chapter 3]):
Find the fluid velocity $\mathbf{u} = \mathbf{u}(\mathbf{x}, t) : \Omega_{\mathrm{f}} \times \mathbb{R}^+ \to \mathbb{R}^3$, the pressure $p = p(\mathbf{x}, t) : \Omega_{\mathrm{f}} \times \mathbb{R}^+ \to \mathbb{R}$, and the solid displacement $\mathbf{d} = \mathbf{d}(\mathbf{x}, t) : \Omega_{\mathrm{s}} \times \mathbb{R}^+ \to \mathbb{R}^3$ such that

$$
\begin{cases}
\rho_{\mathrm{f}} \partial_t \mathbf{u}|_{\mathcal{A}} + \rho_{\mathrm{f}} (\mathbf{u} - \mathbf{w}) \cdot \nabla\mathbf{u} - \nabla \cdot \boldsymbol{\sigma}_{\mathrm{f}} = \mathbf{0} & \text{in} \quad \Omega_{\mathrm{f}}(t), \\
\nabla \cdot \mathbf{u} = 0 & \text{in} \quad \Omega_{\mathrm{f}}(t), \\
\rho_{\mathrm{s}} \partial_{tt} \mathbf{d} - \nabla \cdot \boldsymbol{\Pi} = \mathbf{0} & \text{in} \quad \Omega_{\mathrm{s}}, \\
\mathbf{d} = \mathbf{h} & \text{on} \quad \Gamma_{\mathrm{out}},
\end{cases}
\tag{2}
$$

with the interface coupling conditions

$$
\begin{cases}
\mathbf{d}_{\mathrm{f}} = \mathrm{Ext}(\mathbf{d}|_{\Gamma_{\mathrm{FSI}}}), \quad \mathbf{w} = \partial_t \mathbf{d}_{\mathrm{f}} & \text{in } \Omega_{\mathrm{f}}, \\
\mathbf{u} = \partial_t \mathbf{d} & \text{on } \Gamma_{\mathrm{FSI}}(t), \\
\boldsymbol{\Pi}\mathbf{n}_{\mathrm{s}} = -J_{\mathrm{f}} \boldsymbol{\sigma}_{\mathrm{f}} (\boldsymbol{F}_{\mathrm{f}})^{-\mathrm{T}} \mathbf{n}_{\mathrm{f}} & \text{on } \Gamma_{\mathrm{FSI}}.
\end{cases}
\tag{3}
$$

The initial conditions are: $\mathbf{u}(0) = \mathbf{0}$, $\mathbf{d}(0) = \mathbf{0}$ and $\partial_t \mathbf{d}(0) = \mathbf{0}$; ρ_{f} and ρ_{s} represent the fluid and solid densities, respectively, $\partial_t|_{\mathcal{A}}$ the ALE time derivative, $\boldsymbol{\sigma}_{\mathrm{f}} =$

$\boldsymbol{\sigma}_{\mathrm{f}}(\mathbf{u}, p) \stackrel{\text{def}}{=} -p\mathbf{I} + 2\mu\boldsymbol{\epsilon}(\mathbf{u})$ the fluid Cauchy stress tensor, μ the fluid dynamic viscosity, $\boldsymbol{\epsilon}(\mathbf{u}) \stackrel{\text{def}}{=} 1/2 \left(\nabla\mathbf{u} + \nabla\mathbf{u}^{\mathrm{T}}\right)$ the strain rate tensor, $\boldsymbol{\Pi} = \boldsymbol{\Pi}(\mathbf{d})$ the first Piola–Kirchhoff stress tensor of the structure, $\boldsymbol{F}_{\mathrm{f}} \stackrel{\text{def}}{=} \nabla\mathcal{A}$ the fluid domain gradient of deformation and $J_{\mathrm{f}} \stackrel{\text{def}}{=} \det \boldsymbol{F}_{\mathrm{f}}$ the Jacobian; $\mathbf{n}_{\mathrm{f}}$ and $\mathbf{n}_{\mathrm{s}}$ are, respectively, the outward unit normals to the fluid and solid domains. The displacement field $\mathbf{h}$ is reconstructed from a suitable interpolation in space and time of some registration point on the outer surface Γ_{out} (cf. [20]).

In the linearized St. Venant–Kirchhoff model the Piola tensor is approximated as:

$$\boldsymbol{\Pi} \approx \lambda \mathrm{tr}(\boldsymbol{\epsilon}_{\mathrm{s}})\mathbf{I} + 2\mu_{\mathrm{s}}\boldsymbol{\epsilon}_{\mathrm{s}},$$

with $\boldsymbol{\epsilon}_{\mathrm{s}} = 1/2 \left(\nabla\mathbf{d} + \nabla\mathbf{d}^{\mathrm{T}}\right)$ and λ and μ_{s} the Lamé coefficients. Finally, the harmonic extension problem associated to the operator $\mathrm{Ext}(\cdot)$ reads: Find $\mathbf{d}_{\mathrm{f}} = \mathbf{d}_{\mathrm{f}}(\mathbf{x}, t) : \Omega_{\mathrm{f}} \times \mathbb{R}^{+} \to \mathbb{R}^{3}$ such that

$$\begin{cases} -\Delta\mathbf{d}_{\mathrm{f}} = \mathbf{0}, & \text{in } \Omega_{\mathrm{f}}, \\ \mathbf{d}_{\mathrm{f}} = \mathbf{d}, & \text{on } \Gamma_{\mathrm{FSI}}. \end{cases} \qquad (4)$$

One-dimensional models. The entire arterial system can be modelled as a network of 1D models, each one characterized by a circular cross-section (eventually narrowed along the axial direction) and a viscoelastic arterial wall (e.g. [6, 7, 21]). Such models have proven to be able to provide useful information under physiological and pathophysiological conditions, and therefore give insight about the main characteristics that lead to the interplay among physical phenomena taking place in the systemic arteries.

For each cross-section $S(t, z)$, let us define the state variables

$$A(t, z) = \int_{S(t,z)} d\sigma, \qquad \text{(cross-sectional area)}$$

$$Q(t, z) = \int_{S(t,z)} u_z(t, z)\, d\sigma, \qquad \text{(flow rate)}$$

$$\bar{p}(t, z) = \frac{1}{A(t, z)} \int p(t, z)\, d\sigma. \qquad \text{(averaged pressure)}$$

$$(5)$$

Their evolution is governed by the following system of hyperbolic equations derived in [8]

$$\begin{cases} \dfrac{\partial A}{\partial t} + \dfrac{\partial Q}{\partial t} = 0, \\ \dfrac{\partial Q}{\partial t} + \dfrac{\partial}{\partial z}\left(\alpha \dfrac{Q^2}{A}\right) + \dfrac{A}{\rho}\dfrac{\partial \bar{p}}{\partial z} + K_R \dfrac{\partial Q}{\partial A} = 0. \end{cases} \qquad (6)$$

Here K_R is a resistance parameter accounting for fluid viscosity and α is the Coriolis coefficient. In order to close the system, an additional equation relating the averaged pressure with the other unknowns Q and A is needed. Considering only the elastic and viscoelastic contributions (as all the other terms are negligible in a cardiovascular setting)

the following expression for the pressure-area relation can be derived [13]:

$$\bar{p} - p_{\mathrm{ext}} = \beta \left(\sqrt{\frac{A}{A^0}} - 1\right) + \frac{\gamma}{A\sqrt{A}}\frac{\partial A}{\partial t}, \qquad (7)$$

with

$$\beta := \sqrt{\frac{\pi}{A^0}}\frac{hE}{1 - \nu^2}, \quad \gamma := \frac{T \tan\phi}{4\sqrt{\pi}}\frac{hE}{1 - \nu^2}, \qquad (8)$$

p_{ext} and A^0 being the external pressure of the tissues on the vessel walls and the area of the cross-section of the vessel in the pre-stressed configuration, respectively. The vessel wall is characterized by a thickness h, an elastic Young modulus E and a Poisson coefficient ν. Finally the parameters T and ϕ are the characteristic time (usually taken equal to the systolic period) and the so-called viscoelastic angle, respectively.

In this work we use the data of the arterial network provided in [21] (Figure 2 and Table 2); the model includes 103 elements – 4 coronary, 24 aortic, 51 cerebral, 10 in the arms, and 14 in the legs.

Lumped parameter models. In order to complete our geometrical multiscale model it is necessary to include two additional elements: the peripheral circulation and the ventricular valves. Both of them are here described by means of lumped parameter models.

The peripheral circulation is taken into account by coupling the terminal nodes of the 1D network to windkessel models. In particular, here we use the three element RCR windkessel model described in Figure 1 which leads to the
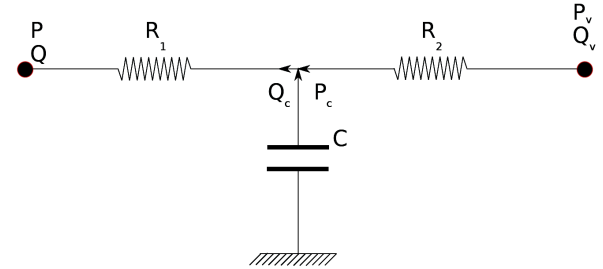
Figure 1 Three element RCR windkessel model used at the terminal nodes of the arterial network.

following equation (see [21])

$$\frac{dP}{dt} = -\frac{P}{CR_2} - \frac{R_1 + R_2}{CR_2}Q - R_1\frac{dQ}{dt} + \frac{P_v}{CR_2}, \quad (9)$$

P and Q are the pressure and the flow rate at the terminal node, respectively, $P_v = 666$ Pa [5 mmHg] is the venous pressure, while R_1, R_2, and C model the resistances and the compliance of the peripheral circulation.

For the ventricular valves, different lumped parameter models have been proposed in literature (see [1, Chapter 7] for a review). Similarly to [1, 7], the valves are here defined as ideal diodes that allow the blood to flow in only

one direction, preventing its backflow. In order to present the model, let us consider for the sake of simplicity the aortic valve surface (AV) and define on its two sides (ventricular and aortic) the mean normal stress Σ and the flow rate Q. On the ventricular side (VS), these quantities are computed as:

$$\Sigma_{\mathrm{VS}}(t) := \frac{1}{|\Gamma_{\mathrm{AV}}|} \int_{\Gamma_{\mathrm{AV}}} (\boldsymbol{\sigma}_{\mathrm{f}}(t) \cdot \mathbf{n}) \cdot \mathbf{n} \, d\Gamma,$$
$$Q_{\mathrm{VS}}(t) := \int_{\Gamma_{\mathrm{AV}}} \mathbf{u}(t) \cdot \mathbf{n} \, d\Gamma, \tag{10}$$

while for aortic side (AS) they are defined by:

$$\Sigma_{\mathrm{AS}}(t) := \bar{p}(t)|_{\mathrm{AV}} + p_{\mathrm{ref}}, \quad Q_{\mathrm{AS}}(t) := Q(t)|_{\mathrm{AV}}, \tag{11}$$

where $p_{\mathrm{ref}} = 10$ kPa [75 mmHg] is the reference pressure. The state of the valve (open or closed) is defined according to the values of these scalar quantities and the resulting lumped parameter models is based on the following two physiological considerations:

1. if the valve is closed and $\Sigma_{\mathrm{VS}} > \Sigma_{\mathrm{AS}}$, then it opens;

2. if the valve is open ans $Q_{\mathrm{VS}} < 0$ (i.e., when backflow from the aorta is observed), then it closes.

Despite the fact that the valve operates only on the averaged/integrated quantities of the flow field, we have observed little unphysiological residual flow through it during the simulation of the diastolic phase. In any case, the modularity of our geometrical multiscale model allows for a very simple incorporation of more advanced models, e.g. for the mitral valve, since all models, be they 0D, 1D, 3D, or 3D FSI, are implemented as subsystems that are coupled together with the same methodology.

In order to prescribe the displacement of the ventricle, while still obtaining physiological pressure values for the blood inside it, we need to model both the mitral valve and the pressure inside the left atrium. As a first approximation, the latter can be taken as constant. The mitral valve is simulated with the same diode model as the aortic valve. The mitral inflow during the diastole is prescribed as an integrated flux Q_{MV} related to the pressure difference between the left ventricle pressure and the left atrium according to the linear law

$$Q_{\mathrm{MV}} = \begin{cases} \dfrac{p_{\mathrm{LA}} - p_{\mathrm{LV}}}{R_{\mathrm{MV}}} & \text{if } p_{\mathrm{LA}} > p_{\mathrm{LV}} \\ 0 & \text{otherwise}, \end{cases} \tag{12}$$

where $R_{\mathrm{MV}} = 1$ Pa·s/cm^3 is the flow resistance of the mitral valve that we tuned empirically to fit our model parameters. Thus we make no assumption of the flow profile at the mitral valve relying on unfounded assumptions of fully-developed flow. This correctly captures the E-wave of the diastolic phase, as the mitral inflow during the early diastolic phase is believed to be mainly driven by the suction created by the expansion of the left ventricle [26]. In order to model the A-wave, i.e., the secondary flow peak

caused by the contraction of the left atrium that occurs at the latter part of the diastolic phase, it is necessary to incorporate a further model with nonconstant atrial pressure and/or the contraction of the left atrium. We will address this aspect in a future work.

Numerical approximation

Three-dimensional models. The 3D FSI problem is discretized in time with a geometry-convective explicit scheme (GCE) [3], i.e., the fluid computational domain and the convective field are extrapolated from the previous time iteration. The Navier–Stokes equations therefore reduce to the linear Oseen equations, and the 3D FSI problem at each time level is linear. The Oseen equations are discretized in space by $\mathbb{P}_1/\mathbb{P}_1$ finite elements that are stabilized with the interior penalty (IP) method [2]. In this work we do not consider any turbulence model, even if in the physiological case a transition to turbulence takes place during the diastolic. In our experience the IP stabilization is sufficient to avoid stability problems related to the onset of turbulence.

The structural equations are also linear and require no special treatment. Since the geometry is treated explicitly, the fluid computational domain $\Omega_{\mathrm{f}}(t^{k+1})$ is computed by using $\mathbf{d}_{\Gamma_{\mathrm{s}}}^k$ as boundary condition in (4). Thus the coupled 3D FSI model after discretization gives at each timestep t^{k+1} a monolithic linear system to solve for

$$\begin{bmatrix} \mathrm{F}_{\mathrm{ff}} & \mathrm{F}_{\mathrm{f}\Gamma} & & & \\ \mathrm{F}_{\Gamma\mathrm{f}} & \mathrm{F}_{\Gamma\Gamma} & & & \mathrm{I} \\ & & \mathrm{S}_{\mathrm{ss}} & \mathrm{S}_{\mathrm{s}\Gamma} & \\ & & \mathrm{S}_{\Gamma\mathrm{s}} & \mathrm{S}_{\Gamma\Gamma} & -\mathrm{I} \\ & -\mathrm{I} & & \mathrm{I}/\Delta t & \end{bmatrix} \begin{bmatrix} \mathbf{y}^{k+1} \\ \mathbf{y}_\Gamma^{k+1} \\ \mathbf{d}^{k+1} \\ \mathbf{d}_\Gamma^{k+1} \\ \lambda^{k+1} \end{bmatrix} = \begin{bmatrix} \mathbf{f}_{\mathrm{f}}^{k+1} \\ \mathbf{0} \\ \mathbf{f}_{\mathrm{s}}^{k+1} \\ \mathbf{0} \\ \mathbf{d}_\Gamma^k/\Delta t \end{bmatrix}, \tag{13}$$

where $\mathbf{y}^k := (\mathbf{u}^k, p^k)$ denotes the fluid variables, vectors with subindices Γ represent all the variables on the fluid-structure interface Γ_{FSI}, λ^k is a Lagrange multiplier that corresponds to the force transferred from fluid to structure, and the blocks $\mathrm{F}_{\alpha\beta}$ and $\mathrm{S}_{\alpha\beta}$ correspond to the sub-blocks of the finite element matrices of the fluid and structure problems respectively. The 3D FSI system (13) is solved by a GMRES method preconditioned by overlapping algebraic Schwarz preconditioners based on an inexact block factorization of the system in the block-composed form. The solution strategy of the monolithic 3D FSI system (13) is detailed in [3].

One-dimensional models. By inserting (7) into (6), after some manipulations, we reach a system of differential equations that can be written in a classical conservative form as follows

$$\frac{\partial \mathbf{U}}{\partial t} + \frac{\partial \mathbf{F}(\mathbf{U})}{\partial z} + \mathbf{S}(\mathbf{U}) = 0, \tag{14}$$

where $\mathbf{U}$ are the conservative variables, $\mathbf{F}$ the corresponding fluxes, and $\mathbf{S}$ represents the source terms. Following

[6] we solve problem (14) by using an operator splitting technique that takes a fully explicit second-order Taylor-Galerkin step for the elastic part of the operator, followed by a viscoelastic correction step. A full description of the solution method is given in [13].

Geometrical multiscale algorithms

The coupling between all the elements in the network (including all the 1D arterial segments and the 3D FSI heart) is provided by imposing at each interface the conservation of the flow rate $Q_{c,m}$ and the equilibrium of the normal stresses $\Sigma_{c,m}$:

$$\forall c = 1, \ldots, \mathcal{C} : \begin{cases} \sum_{m=1}^{\mathcal{M}_c} Q_{c,m} = 0, \\ \Sigma_{c,1} = \Sigma_{c,m}, \quad \forall m = 2, \ldots, \mathcal{M}_c, \end{cases}$$
(15)

where $\mathcal{C}$ is the total number of coupling interfaces, and $\mathcal{M}_c$ is the number of models coupled by the c-th coupling interface (see Figure 2). To satisfy the set of equations (15),
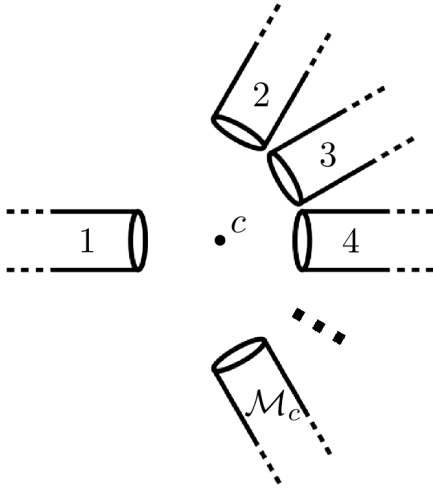
Figure 2 General configuration for the c-th coupling between $\mathcal{M}_c$ models.

we can use different coupling strategies corresponding to the imposition of different quantities on the boundaries. In other words, we can set up each subproblem with different combinations of boundary data over the coupling interfaces. Some examples are provided in [14].

The global coupled system is then solved by using a classical nonlinear Richardson strategy until convergence to a suitable tolerance has been achieved. In particular, we use a quasi-Newton iterative technique, where we compute the approximate Jacobian matrix of the coupled problem and then we provide a correction at each iteration using a Broyden update strategy. This approach leads to a convergent coupling algorithm even when more than one hundred constituent models were coupled together; in particular we reach the convergence in few iterations (around 5, with a tolerance of 1e-6 and without topological changes) after

an initial buildup phase. In case of topological changes of the system between two time steps (such as the opening or closing of the aortic valve), we are forced to discard the previous Broyden approximant for the Jacobian of the coupled problem and we therefore proceed with a reinitialization of the Jacobian matrix by performing one inexact-Newton step. This causes an increase of the average number of iterations required by the Broyden method, due to the fact that all the previous updates of the Jacobian are lost, even those unrelated to the change of the topology. Therefore a better approach would be to reinitialize just the lines/columns directly affected by the topological change. This and other improvements will be discussed in future works. More details about the coupling algorithms are provided in [14].

Results

The idealized heart is modelled as an ellipsoid with two valves on the top, the larger one being the mitral valve and the smaller one the aortic valve. The ellipsoid is discretized using two tetrahedral meshes. The meshes are matching at the interface. The mesh for the fluid consists of 41,550 tetrahedral elements (unstructured) with 7,913 vertices, and the mesh for the structure consists of 28,080 tetrahedral elements (structured) with 6,356 vertices. In Figure 3 we display a baseline mesh for the fluid and structure parts respectively. These meshes are refined in order to obtain the meshes used in the actual simulations. At the top of the fluid mesh the two circular valve surfaces can be seen.

As a first test of our proposed multiscale model, we prescribe idealized inputs for the left ventricle, mainly the atrial pressure $p_{\text{LA}}(t)$ and a time-varying normal force $g_{\text{epi}}(t)$ acting on the epicardium to simulate a heart undergoing electromechanical activation and deformation. The applied force is shown Figure 4 and it can be identified using the time-varying elastance method of Suga et al [25]. The goal is to demonstrate that our multiscale model is passive and that it achieves a periodic state after a few heartbeat cycles. We are also able to obtain simulation results of flow rate and blood pressure measured at down-circulation that are within the physiological range. In a future work we aim to consider an applied displacement of the structure obtained from a set of medical images that could be used to obtain more realistic patient-specific ventricle behavior.

Model parameters and inputs are described in Table 1 for reference. The numerical simulation of the left ventricle is initialized with $\mathbf{u} \equiv 0$, $p \equiv 0$ and with both valves closed at the end-of-diastole. A reference pressure of 10 kPa [75 mmHg] is imposed at the aortic valve, which means that the pressure rises until it reaches a physiological level at around $t = 0.04$ s and the aortic valve opens. The simulation is allowed to proceed until $t = 4.8$ s, i.e., six full heartbeats, in order to reach the physiological pressure level. The time step for the 3D FSI simulation is $\Delta t = 0.001$ s.

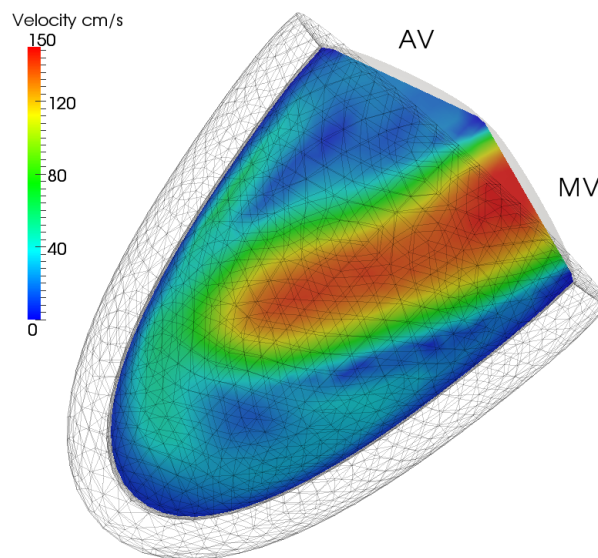Snapshots of the velocity field $|\mathbf{u}|$ and the vorticity field
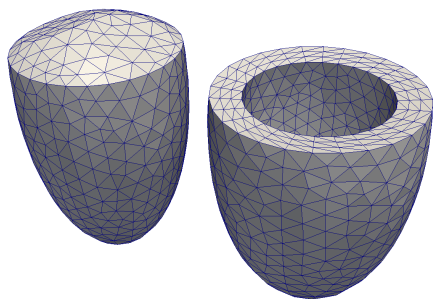
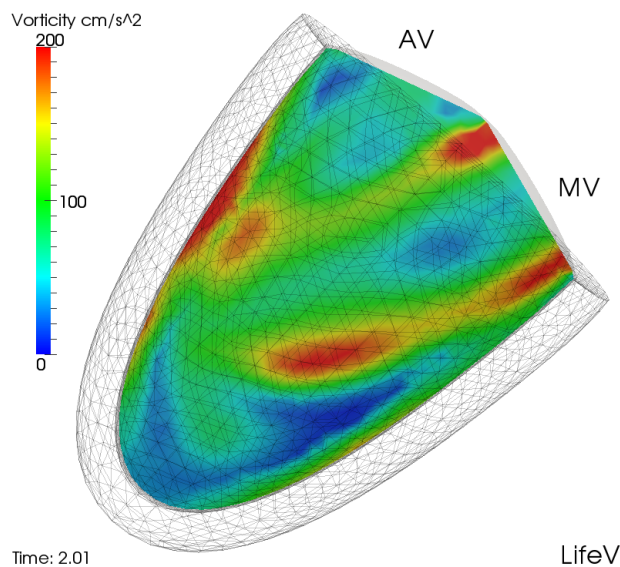**Figure 3 Coarse finite element meshes for the fluid domain (left) and the elastic pseudo-structure domain (right).**
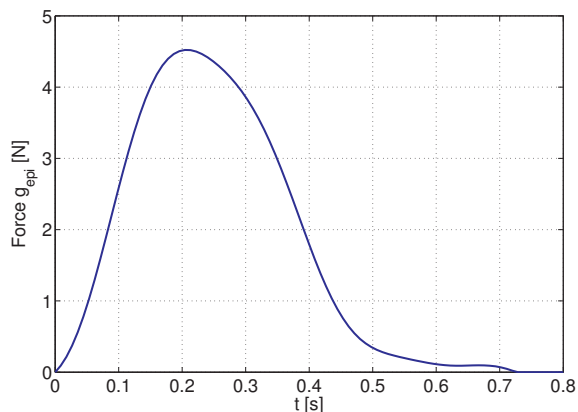
Figure 4 Time-varying normal force applied on the epicardium to simulate deformation of the heart.

Figure 5 Left ventricle, absolute value of the velocity of the flow in the long axial plane during the early diastole.

Figure 6 Left ventricle, absolute value of the vorticity of the flow in the long axial plane during the early diastole.

$\omega := |\nabla \times \mathbf{u}|$ inside the ventricle during the early diastole are shown in Figure 5 and Figure 6. The velocity profile is strongly nonparabolic in the early diastole and only develops into parabolic inflow during the middle part of the diastole. With the model used we did not capture the A-wave effect of the atrial contraction. Despite the lack of valve leaflets in our 3D FSI model, two vortices are created on both sides of the mitral valve that travel across the length of the ventricular cavity and slowly dissipate in the base of the ventricle during the late diastole. Thus even with such a relatively idealized model it may be possible in the future to make qualitative evaluations of vortex patters between healthy and pathological left ventricles along the lines presented in [10].

All simulations were performed on four nodes with eight cores each of the Intel Nehalem cluster *Antares* at the EPFL. The simulation of one heartbeat takes approximately 25 hours of wall-clock time. The number of nonlinear iterations taken by the Broyden/Newton schemes for coupling all the models together at each time step is shown in Figure 7. The coupling tolerance was fixed at 1e-6. We observe that, after an initial transient phase where the model starts from rest and tries to reach the physiological conditions, the Broyden method takes consistently 5-15 iterations per time step except whenever the aortic valve opens and a fallback to the Newton scheme is necessitated. In order for the multiscale coupling algorithm to be practical it is vital that the number of nonlinear iterations grows
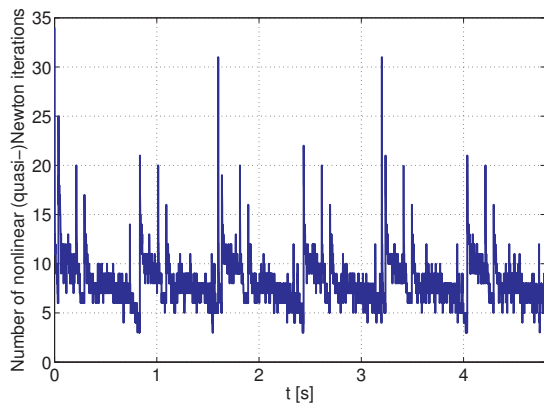
Figure 7 Number of nonlinear quasi-Newton iterations required for the coupling of the multiscale model.

sublinearly as a function of the number of constituent models, and we observe such behavior here.

The upper part of the Wiggers diagram in Figure 8 displays the simulated blood pressure inside the left ventricle, base of the ascending aorta, and left atrium (prescribed input to the model). Due to the idealized on/off valve we use here there is no backflow through the mitral valve during the end-diastole. This could be rectified by incorporating a more involved 0D model for the mitral valve e.g. along the lines presented in [1, 11]. Isovolumic contraction and relaxation phases can be observed from the volume diagram. Volumetric quantities of the left ventricle obtained during the 3rd heartbeat are EDV = 165.4 ml, ESV = 89.7 ml, and the cardiac output CO = 5.68 l/min. The low ejection fraction (45.8%) is due to the unphysiological deformation applied to the ventricle that does not account for torsion and axial contraction.

In Figure 9 we show the simulated flow rate and pressure at various aortic branches of the 1D network. The results are in close agreement to the ones obtained using [21] with a prescribed cardiac output. Some features of note include the dicrotic notch visible in the pressure function of the ascending aorta at $t = 0.2$ s, which corresponds to the closure of the aortic valve, and the backflow in the abdominal aorta during the early diastole. In order to achieve smooth nonoscillatory profiles it is necessary to incorporate in the models both the viscoelastic term for the 1D arterial walls as well as the RCR windkessel elements for the terminals modelling the peripheral circulation. In our experience neglecting either of these two aspects from the multiscale model leads to excessively oscillating profiles in both the flow rate and blood pressure. Our multiscale model reaches a nearly-periodic pressure level in as few as three heartbeats.

A visualization of the arterial tree as a 1D network is represented Figure 10. The thickness of the 1D sections is not in scale to their length (in order to enhance the visualization), and their positioning is purely visual.

Conclusions

We have presented a multiscale model of an idealized left ventricle coupled to a 1D viscoelastic arterial tree for sim-
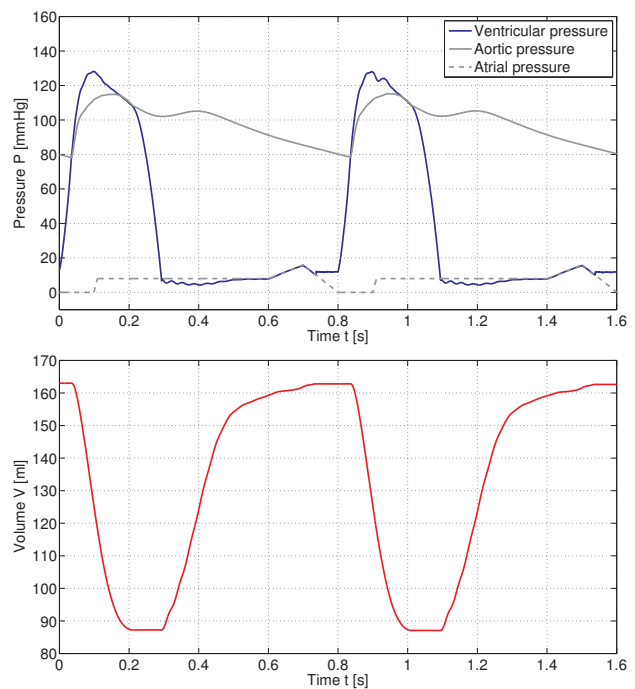
Figure 8 Left ventricle, simulated ventricular pressure and volume during the 5th and 6th heartbeat of the simulation.
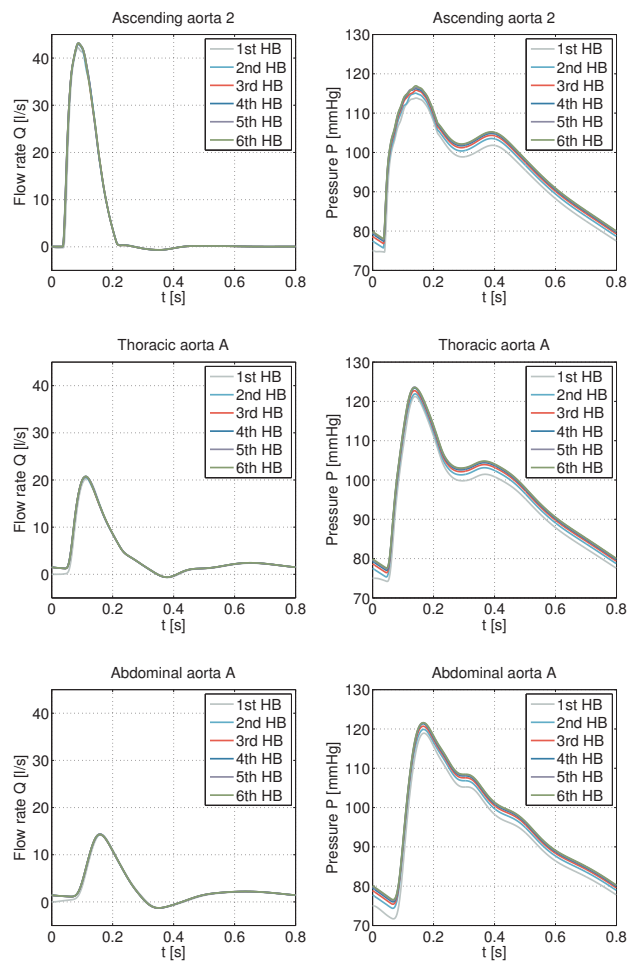
Figure 9 Aortic branches, flow rate Q and pressure P in various aortic arteries. Branch names are taken from [21].
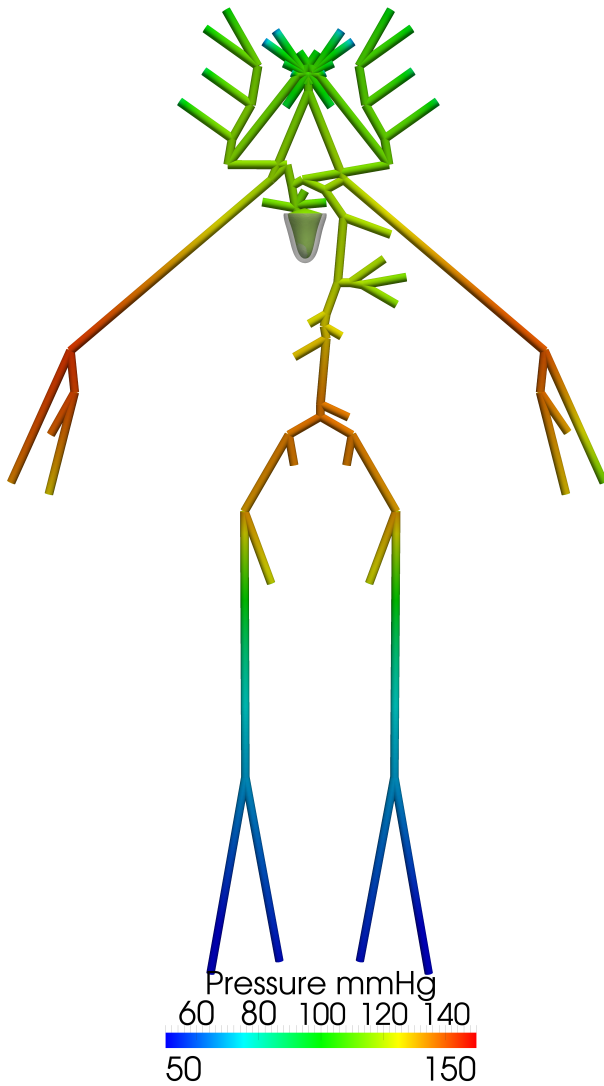
Pressure mmHg
60 80 100 120 140
50   150

Figure 10 Arterial tree, propagation of the pressure wave during late systole. Positioning of 1D network purely visual.

Table 1 Parameter values used in the numerical simulations.

g_{epi}	Force on the epicardium (peak)	4.7 N
E_s	Young modulus of pseudo-structure	0.7 MPa
ν_s	Poisson ratio of pseudo-structure	0.4
ρ_s	Density of elastic pseudo-structure	1.2 g/cm^3
p_{LA}	Left atrial pressure	1–2 kPa
p_{VE}	Venous pressure	0.66 kPa
R_{MV}	Mitral valve resistance	1 Pa·s/cm^3
ρ_f	Density of blood	1.04 g/cm^3
ν_f	Dynamic viscosity of blood	0.035 g·s/cm
σ_{ref}	Reference pressure at aortic valve	10 kPa
	Heart rate	75 bpm
	Simulation time	4.8 s

ulating the pre- and post-surgical conditions of a pathological heart and its effect on the cardiac output. Key ingredients included (i) a scalable parallel library for solving the 3D FSI system for the left ventricle and the 1D hyperbolic system for flow in compliant arteries, and (ii) a general and robust coupling framework for heterogeneous models into one large geometrical multiscale model. While 1D and lumped parameter models are usually sufficient to simulate the principal features of blood flow in the human cardiovascular system, in areas where the geometry of the vessels has a strong effect on the flow it is necessary to use fully 3D models with fluid-structure interaction effects. One also has to provide a method for coupling together dimensionally heterogeneous models.

Our multiscale model reached a physiological pressure level in 3-4 heartbeats, demonstrating that even an idealized left ventricle is able to produce realistic flow patterns and simulate some basic principles of blood flow in the major arteries. In the future we aim to assimilate patient-specific ventricle data and explore the effects of ventricular surgery on the cardiac output (cf. also [20]). To achieve this goal it is necessary to further refine the models being used and to eventually consider a full closed-loop circulation model. Therefore, the geometrical multiscale modelling and coupling framework must be implemented in a way that is highly modular and extensible. The coupling of constituent models should be robust and efficient and the number of nonlinear iterations taken at each time step should not grow exceedingly as the size of the multiscale model grows. We have presented results that indicate the proposed framework satisfies these requirements. The final goal is to provide a toolbox of models that can be used by medical professionals with modest training in numerical methods and no experience in C++ programming for experimentation and development of new multiscale models for investigating specific clinical applications in the treatment of cardiovascular disease.

Acknowledgements

References

[1] M. Astorino. *Interaction fluide-structure dans le système cardiovasculaire. Analyse numérique et simulation*. PhD thesis, Université Pierre et Marie Curie Paris VI, 2010.

[2] E. Burman, M. Fernández, and P. Hansbo. Continuous interior penalty finite element method for Oseen's equations. *SIAM J. Numer. Anal.*, 44(3):1248–1274, 2006.

[3] P. Crosetto, S. Deparis, G. Fourestey, and A. Quarteroni. Parallel algorithms for fluid-structure interaction problems in haemodynamics. *SIAM J. Sci. Comput.*, 33(4):1598–1622, 2011.

[4] P. Crosetto, P. Reymond, S. Deparis, D. Kontaxakis, N. Stergiopulos, and A. Quarteroni. Fluid-structure interaction simulation of aortic blood flow. *Comput. Fluids*, 43(1):46 – 57, 2011.

[5] S. Deparis. Review of LifeV – a parallel finite element library. http://www.lifev.org, In preparation.

[6] L. Formaggia, D. Lamponi, and A. Quarteroni. One-dimensional models for blood flow in arteries. *J. Engr. Math.*, 47(3):251–276, 2003.

[7] L. Formaggia, D. Lamponi, M. Tuveri, and A. Veneziani. Numerical modeling of 1D arterial networks coupled with a lumped parameters description of the heart. *Comput. Meth. Biomech. Biomed. Eng.*, 9(5):273–288, 2006.

[8] L. Formaggia, F. Nobile, A. Quarteroni, and A. Veneziani. Multiscale modelling of the circolatory system: a preliminary analysis. *Comp. Vis. Science*, 2:75–83, 1999.

[9] L. Formaggia, A. Quarteroni, and A. Veneziani. Multiscale models of the vascular system. *In: Formaggia, L., Quarteroni, A., and Veneziani, A. (Eds.), Cardiovascular Mathematics – Modeling and simulation of the circulatory system, Springer-Verlag*, 2009.

[10] G. Hong, G. Pedrizzetti, G. Tonti, P. Li, Z. Wei, J. Kim, A. Baweja, S. Liu, N. Chung, H. Houle, et al. Characterization and quantification of vortex flow in the human left ventricle by contrast echocardiography using vector particle image velocimetry. *JACC Cardiovasc. Imaging*, 1(6):705, 2008.

[11] T. Korakianitis and Y. Shi. A concentrated parameter model for the human cardiovascular system including heart valve dynamics and atrioventricular interaction. *Med. Eng. Phys.*, 28(7):613–628, 2006.

[12] S. Kovács, D. McQueen, and C. Peskin. Modelling cardiac fluid dynamics and diastolic function. *Phil. Trans. R. Soc. Lond. A*, 359:1299–1314, 2001.

[13] A. Malossi, P. Blanco, and S. Deparis. A two-level time step technique for the partitioned solution of one-dimensional arterial networks. Technical report, EPFL-SB-MATHICSE-CMCS, 2011.

[14] A. Malossi, P. Blanco, S. Deparis, and A. Quarteroni. Algorithms for the partitioned solution of weakly coupled fluid models for cardiovascular flows. *To appear in Int. J. Num. Meth. Biomed. Engng.*, 2011.

[15] P. Moireau, X. Nan, M. Astorino, C. Figueroa, D. Chapelle, C. Taylor, and J.-F. Gerbeau. External tissue support and fluid-structure simulation in blood flows. *Biomech. Model Mechanobiol.*, 2011. Published online.

[16] M. Nash and P. Hunter. Computational mechanics of the heart. *J. Elasticity*, 61:113–141, 2000.

[17] F. Nobile. *Numerical approximation of fluid-structure interaction problems with application to haemodynamics*. PhD thesis, École Polytechnique Fédérale de Lausanne, 2001.

[18] F. Nobile, A. Quarteroni, and R. Ruiz-Baier. Numerical simulation of an active strain electromechanical model for cardiac tissue. Technical Report 163380, EPFL-SB-MATHICSE-CMCS, 2011.

[19] M. Piccinelli, L. Mirabella, T. Passerini, E. Haber, and A. Veneziani. 4D Image-Based CFD Simulation of Compliant Blood Vessel. Technical Report TR-2010-027, Emory University, 2010.

[20] V. Positano, M. Marinelli, E. Caiani, M. Santarelli, A. Pingitore, A. Redaelli, M. Lombardi, L. Landini, and O. Parodi. A software framework for global and regional quantitative assessment of myocardial necrosis by cardiac magnetic resonance. *Proc. Intl. Conf. eChallenges (P. Cunningham and M. Cunningham, Eds)*, 2010.

[21] P. Reymond, F. Merenda, F. Perren, D. Rüfenacht, and N. Stergiopulos. Validation of a one-dimensional model of the systemic arterial tree. *Am. J. Physiol.-Heart C*, 297(1):H208, 2009.

[22] S. Rossi, R. Ruiz-Baier, L. Pavarino, and A. Quarteroni. An orthotropic active strain model in cardiac mechanics: a numerical study. *Submitted*, 2011.

[23] J. Sainte-Marie, D. Chapelle, R. Cimrman, and M. Sorine. Modeling and estimation of the cardiac electromechanical activity. *Comput. Struct.*, 84:1743–1759, 2006.

[24] Y. Shi, P. Lawford, and R. Hose. Review of zero-d and 1-d models of blood flow in the cardiovascular system. *Biomed. Eng. Online*, 10(1):33, 2011.

[25] H. Suga, K. Sagawa, and A. Shoukas. Load independence of the instantaneous pressure-volume ratio of the canine left ventricle and effects of epinephrine and heart rate on the ratio. *Circ. Res.*, 32:314–322, 1973.

[26] M. Thiriet and K. Parker. Physiology and pathology of the cardiovascular system: a physical perspective. *In: Formaggia, L., Quarteroni, A., and Veneziani, A. (Eds.), Cardiovascular Mathematics – Modeling and simulation of the circulatory system, Springer-Verlag*, 2009.